Layer-dependent anisotropic electronic structure of freestanding quasi-two-dimensional MoS_2

Jinhua Hong,[1] Kun Li,[2] Chuanhong Jin,[1,*] Xixiang Zhang,[3,†] Ze Zhang,[1] and Jun Yuan[1,4,‡]

[1]*State Key Laboratory of Silicon Materials and School of Materials Science and Engineering, Zhejiang University, Hangzhou, Zhejiang 310027, People's Republic of China*

[2]*Advanced Nanofabrication, Imaging and Characterization Core Lab, King Abdullah University of Science and Technology (KAUST), Thuwal 239955, Kingdom of Saudi Arabia*

[3]*Division of Physical Science and Engineering, King Abdullah University of Science and Technology (KAUST), Thuwal 239955, Kingdom of Saudi Arabia*

[4]*Department of Physics, University of York, Heslington, York, YO10 5DD, United Kingdom*

(Received 14 May 2014; revised manuscript received 14 January 2016; published 29 February 2016)

The anisotropy of the electronic transition is a well-known characteristic of low-dimensional transition-metal dichalcogenides, but their layer-thickness dependence has not been properly investigated experimentally until now. Yet, it not only determines the optical properties of these low-dimensional materials, but also holds the key in revealing the underlying character of the electronic states involved. Here we used both angle-resolved electron energy-loss spectroscopy and spectral analysis of angle-integrated spectra to study the evolution of the anisotropic electronic transition involving the low-energy valence electrons in the freestanding MoS_2 layers with different thicknesses. We are able to demonstrate that the well-known direct gap at 1.8 eV is only excited by the in-plane polarized field while the out-of-plane polarized optical gap is 2.4 ± 0.2 eV in monolayer MoS_2. This contrasts with the much smaller anisotropic response found for the indirect gap in the few-layer MoS_2 systems. In addition, we determined that the joint density of states associated with the indirect gap transition in the multilayer systems and the corresponding indirect transition in the monolayer case has a characteristic three-dimensional-like character. We attribute this to the soft-edge behavior of the confining potential and it is an important factor when considering the dynamical screening of the electric field at the relevant excitation energies. Our result provides a logical explanation for the large sensitivity of the indirect transition to thickness variation compared with that for the direct transition, in terms of quantum confinement effect.

DOI: 10.1103/PhysRevB.93.075440

I. INTRODUCTION

Atomically thin molybdenum disulfide (MoS_2), as a representative member of the emerging two-dimensional (2D) transition-metal dichalcogenides (TMDs) [1,2], has attracted intensive research efforts owing to its unique structure as well as its novel applications in optoelectronics [3–8] and valleytronics [9,10]. It shows a strong layer-dependent electronic structure which changes dramatically at the atomically thin limit. For example, the theoretically predicted transition from an indirect to a direct energy gap [11,12] has been confirmed initially indirectly by the observation of strong photoluminescence (PL) enhancement in the monolayer [13,14] and now directly by angular resolved photoemission spectroscopy (ARPES) [15,16]. The observation of strong chiral pumping effect in the band-gap absorption [9,10] has opened up the possibility of dynamical control of valley-specific carrier density in the monolayer system which lacks inversion symmetry. The realization of vertically stacked heterostructures [17,18] also opens the door to explore new physics and applications through combinations of different atomically thin layers, such as significant extrinsic photoconversion in graphene/TMD/graphene trilayer heterojunction [19].

Despite intense efforts on these novel TMDs, the anisotropic properties of the optical response of these low-dimensional semiconductors, particularly their evolution with the layer thickness, has received much less experimental attention. This is particularly glaring as optical response of bulk MoS_2 itself is known to be already highly anisotropic [20]. Anisotropic electronic excitation plays an important role because of the existence of significant out-of-plane bonding between sulfur and Mo atoms. On the practical level, the out-of-plane optical response is difficult to measure even for bulk MoS_2 and related materials as either thick samples with optical-quality surfaces or large-area layered materials are required for experiments with oblique illumination [20]. Nevertheless, such measurements are extremely useful to understand the complex electronic structure of atomically thin TMDs. For example, it can reveal directly the out-of-plane energy gap which is important for the vertical transport in layer-stacking heterostructures [17] and also complement the partial picture of the electronic structure given by optical absorption [13,14] which usually probes more efficiently the states sensitive to in-plane electric field of the normal incident light. Here we want to emphasize that the periodic band structure of the bulk MoS_2 system will evolve into the "discrete atomic levels" in the out-of-plane direction when the thickness is reduced to atomically thin MoS_2 (0.6 nm–3 nm thickness). For consistence, we will use the term "energy gap" or "optical gap" transitions for the out-of-plane excitation in single or few-layer MoS_2 systems in order to make the correspondence between features in atomic thin films and those in the bulk form.

In this work, we first have utilized the ability to control both the size and direction of the momentum transfer vector in momentum-dependent electron energy-loss spectroscopy

*Corresponding author: chhjin@zju.edu.cn
†xixiang.zhang@kaust.edu.sa
‡jun.yuan@york.ac.uk

(EELS) of atomically thin MoS_2. We characterize the equivalent optical response to reveal the anisotropic properties of the electronic excitations and their layer-thickness dependence. EELS has been long recognized as an alternative nonoptical tool to probe electronic structures of semiconductors and has been used to study the valence electron excitation such as band-gap transition [21,22] and plasmonics [23,24]. In EELS, the momentum transfer vector ($\vec{q} = \vec{k}_i - \vec{k}_f$) plays the role of the polarization vector in optical absorption [25], where $\vec{k}_i$ and $\vec{k}_f$ are the wave vectors of the incident and outgoing electrons, respectively. The angular- (or momentum-) resolved EELS is thus particularly suited to probe the anisotropy of the electronic transitions because the directions of the momentum transfer can range from being parallel to being perpendicular to the incident direction around the characteristic scattering angle ($\theta_E = E/2E_0$) [26], where E is the energy loss and E_0 is the kinetic energy of incident electrons. Our result, taken with the specimen's c axis parallel with the incident beam, can therefore mimic the optical experiments taken both at normal and glancing angles [see Fig. 1(a)]. It has revealed a strong difference between the in-plane and out-of-plane polarized response, and has allowed us to track the changes of underlying electronic structures when analyzed in detail with the reported ARPES results [15,16]. In addition, through spectral analysis we not only provide a direct confirmation of the well-known indirect-to-direct gap transition but also determine directly the monolayer's out-of-plane optical gap (2.4 ± 0.2 eV) which is significantly different from the well-known in-plane gap (1.8 eV) [13] and important to understand energy gap mismatch in vertically stacked heterostructures. The unexpected three-dimensional-like character of the joint density of states (JDOS) of the indirect transition, even in monolayer, has implications on the electronic structure engineering as well as the charge screening effect in MoS_2. Our work also provides a vital experimental check of theoretical calculation [27] of optical spectra at above gap energies, particularly with regard to the layer-thickness dependence as a consequence of quantum confinement effect.

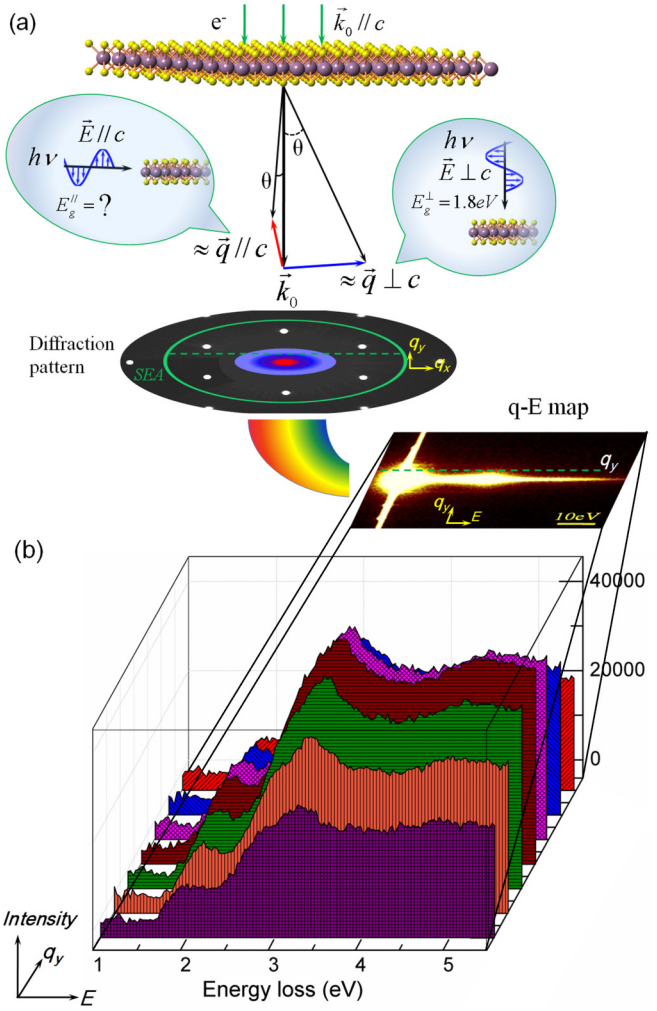

FIG. 1. The experimental setup and the resulting momentum-dependent spectra. (a) Inelastic electron scattering geometry in analogy with polarized optical measuring. The samples in the TEM are atomically thin MoS_2 layers. EELS spectra with in-plane polarization ($\vec{q} \perp c$) dominate the larger-scattering-angle region (blue) and resemble the well-known optical excitation at normal incidence (right inset) onto atomic layers. Whereas, the out-of-plane polarized ($\vec{q} // c$) spectra reside in the small-scattering-angle region (red) in the momentum space, similar to the unexplored grazing-incidence case of optical wave (left inset). (b) Corresponding momentum-dependent spectra extracted from the q-E diagram with q_y along the ΓM direction in (a).

II. METHODS

Atomically thin MoS_2 was prepared through the standard micromechanical exfoliation process, and transferred onto a copper grid with lacey carbon film for TEM observations. No polymer such as polymethyl methacrylate (PMMA) was used during the transfer process, which can substantially decrease the possible contamination.

Monochromated EELS measurements were conducted in a TEM (FEI Titan 60–300) equipped with a Gatan Tridiem 865 spectrometer. This microscope was operated at 60 kV in order to reduce the irradiation damage. The attainable energy resolution is less than 140 meV in the absence of specimens, and this value changes to 0.2 eV under experimental conditions used for MoS_2 monolayers. The convergence semiangle of the incident electron beam was set to be less than $\alpha \sim 0.3$ mrad to yield a nearly parallel illumination. EEL spectra were recorded with the microscope operating in the diffraction mode and a rotation holder was used to choose the specific orientation, similar to that used by Wachsmuth *et al.* [24]. A selected-area aperture with a diameter of 10 μm was used for electron diffraction that corresponds to an illumination area with a diameter of 200 nm on the specimen. The scattering geometry of AREELS was limited by a spectrometer entrance aperture (SEA) with a diameter of 2.5 mm (corresponding to 0.54 $Å^{-1}$). Each q-E diagram was recorded for 3 min. All spectra were collected after zero-loss peak alignment and no detectable energy drift (<0.14 eV) was observed during EELS acquisition.

The valence EEL spectra were acquired from freestanding areas (about 200 nm in size) of high-quality MoS_2 monolayers to avoid substrate effect. Figure 1(a) shows the inelastic scattering geometry with the [0001] zone-axis diffraction pattern of a freestanding monolayer MoS_2 at the normal incidence of the electron beam, i.e., parallel with the

specimen's c axis. The scattering kinetics dictates that the in-plane polarization ($\vec{q}\perp c$) component of inelastic spectra dominates the large-scattering-angle region (blue). This mode resembles the well-known optical excitation at normal incidence [13,14] [right inset in Fig. 1(a)] due to the similarity of the momentum transfer vector and the electric field vector in the transition matrix element for EELS and optical absorption, respectively. The out-of-plane polarized ($\vec{q}//c$) component resides in the small-scattering-angle region (red) in the momentum space, similar to the unexplored grazing-incidence case of optical spectroscopy (left inset). The two regions are separated by the characteristic angle of $\theta_E = E/(2E_0) \sim 0.016$ mrad (or $q_E \sim 3.3 \times 10^{-4}$ Å^{-1}).

Superimposed on the diffraction pattern in Fig. 1 is a (green) ring marking the size of the round SEA used in the measurement. The electron energy-loss spectrometer was operated in the energy-dispersive diffraction mode to produce a q-E map, with the partially angular-integrated energy-loss spectrum in the spectrometer's energy dispersing direction (defined as the q_x direction) while the angular information in the perpendicular direction (defined as the q_y direction) is preserved. The momentum-dependent energy-loss map (the q-E diagram) shown in Fig. 1(a) is obtained by summation of 200 individual 1.0 s drift-corrected measurements to enhance the signal. The q_y direction in Fig. 1(a) is aligned along the ΓM direction using a rotation holder. The momentum-dependent spectra are line plots as a function of q_y as shown in Fig. 1(b). Each line plot is an intensity integration along the q_x direction (the energy dispersing direction) over the momentum transfer range limited by the angular size of SEA. For an incident electron beam traveling down the c axis of a uniaxial crystal, the experimental intensity can be written as [25]

$$I(q_y) = \int_{-\sqrt{q_0^2-q_y^2}}^{\sqrt{q_0^2-q_y^2}} \frac{\mathrm{Im}(\varepsilon_{//})q_E^2 + \mathrm{Im}(\varepsilon_{\perp})\left(q_x^2+q_y^2\right)}{\left|\varepsilon_{//}q_E^2 + \varepsilon_{\perp}\left(q_x^2+q_y^2\right)\right|^2} dq_x \Delta q_y, \tag{1}$$

where $q_0 (= 0.54$ Å$^{-1})$ is the size of the SEA in the momentum transfer space, ε is the complex dielectric function, Δq_y is the corresponding pixel size in the unit of the scattering momentum space in the q_y direction, and the subscripts denote the polarization directions with respect to its surface normal of the sample. Here atomically thin thickness excludes the possible influence from Cerenkov loss [28]. Even in this partially momentum-integrated form, the anisotropy information should still be visible as we demonstrate below.

For the angular and energy ranges we are interested in, we did not notice any significant difference in the spectrum acquired with q_y aligned along the ΓK direction to that along the ΓM direction (Fig. 3). Wachsmuth *et al.* [24] has used a similar q-E mapping approach for graphene, but a specially adopted narrow slit has been used to make the integration over q_x shown in Eq. (1) unnecessary to the first approximation. We notice that in-plane anisotropy in their case was only observed at a high scattering angle of 72 mrad (near the Brillouin zone boundary in graphite at 1.2 Å^{-1}; Ref. [24]), comparable to the angular range of SEA in our case (54 mrad). Thus we believe that in the low-energy-loss region of interest we can treat in-plane anisotropy to be negligible in our case.

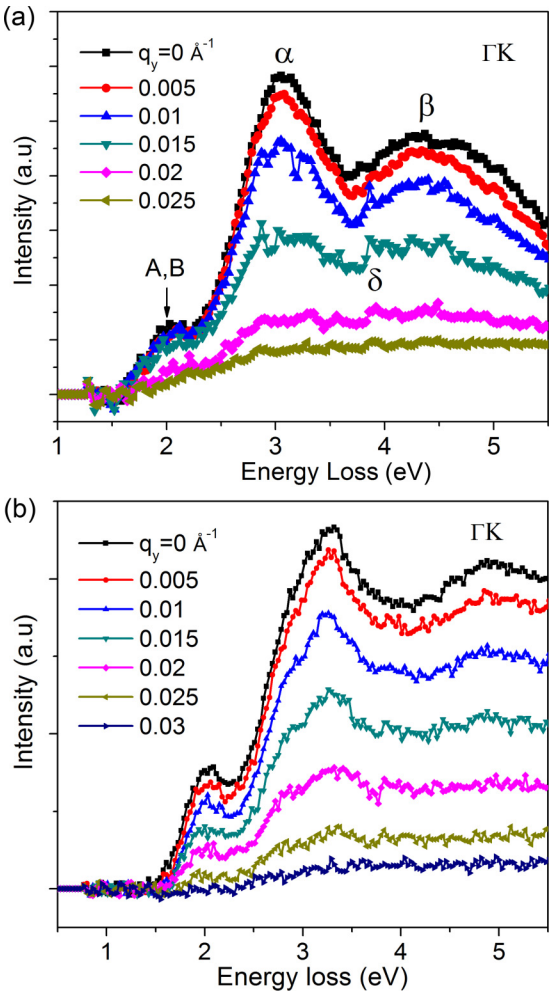

FIG. 2. (a) Angle-resolved low-loss spectra of monolayer MoS_2 with q_y in the ΓK direction. The unit of q_y is Å^{-1}. The weak peak at 2.0 eV is due to the direct transition of A,B excitons, and the strong peaks at 3.1 eV (α) and 4.5 eV (β) result from strong interband transitions (van Hove critical points). (b) Spectra of multilayer MoS_2 with q_y along the ΓK direction. The δ absorption peak arises as q_y increases.

To study the in-plane and out-of-plane anisotropy, we need to resolve the momentum transfer variation in the order of the characteristic angle θ_E (0.016 mrad for energy loss at 2 eV for 60 keV high-energy electrons). As our beam convergence angle is limited to about 0.3 mrad, due to the need to study finite-sized crystals and the presence of any residual beam divergence, one cannot use the traditional method of a linear slit aperture in the EELS to provide momentum resolution in the q_x direction. Instead, we have to work with spectra containing mixed contributions and use the well-known numerical processing method [25,29] to separate the response from the two orientations, as shown later.

III. RESULTS

A. Angle-resolved spectra in atomically thin MoS_2

Figure 2(a) shows the angle-resolved EEL spectra of monolayer MoS_2 extracted from the q-E map with q_y along the

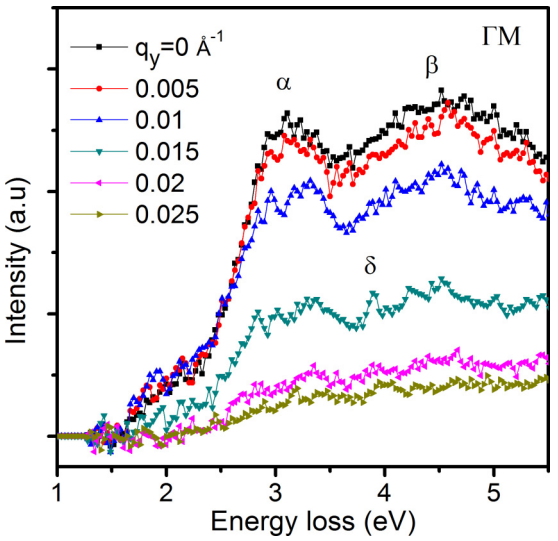

FIG. 3. Momentum-dependent spectra of monolayer MoS_2 with q_y along the ΓM direction. The α peak still splits and an additional δ absorption peak appears as q_y increases.

ΓK direction. The spectra of multilayer MoS_2 with q_y along the ΓK direction behave in a similar way to that shown in Fig. 2(b). Only excitations up to 5 eV are displayed because of our focus on the electronic structure near the absorption edge region. Plasmon excitation at higher energy losses will be discussed in a separate paper. Three noticeable features are observed: a weak transition peaked at 2.0 eV (marked by 'A,B' following the convention of optical spectroscopy [13] which identifies it as spin-orbit split excitons in the KK' direct transition), a group of strong transitions centered at 3.1 eV (α), and a broad peak at 4.5 eV (β). A similar result for EELS in monolayer along the ΓM direction is also shown in Fig. 3, indicating that it is a good approximation to treat the in-plane anisotropy as negligible as we have discussed and reasonable to treat dielectric response as being uniaxial as described by Eq. (1).

B. Angle-integrated spectra of MoS_2 layers with different thicknesses

In Fig. 4, we have collected thickness-dependent spectra from ultrathin MoS_2 to illustrate the joint density of states and quantum confinement effect of electronic transitions as discussed later. Figure 4 shows the fine structures of low-loss spectra from MoS_2 with variable thicknesses. They are obtained by integrating the (q_y, E) map over all q_y to improve the statistics for further spectral analysis.

IV. DISCUSSIONS

A. Anisotropy in atomically thin MoS_2

The momentum-dependent EEL spectra show strong evidence for the in-plane/out-of-plane anisotropy of the electronic transition in the energy range studied. In Fig. 5, we have plotted the intensity variations of the three dominant absorptions (A,B; α; β) with the intensity at q_y, normalized to their values at $q_y = 0$. We expect the out-of-plane component ($\vec{q}//c$) to dominate the spectrum at $q_y = 0$ and the in-plane ($\vec{q}\perp c$) component to dominate at large q_y. Although the integration

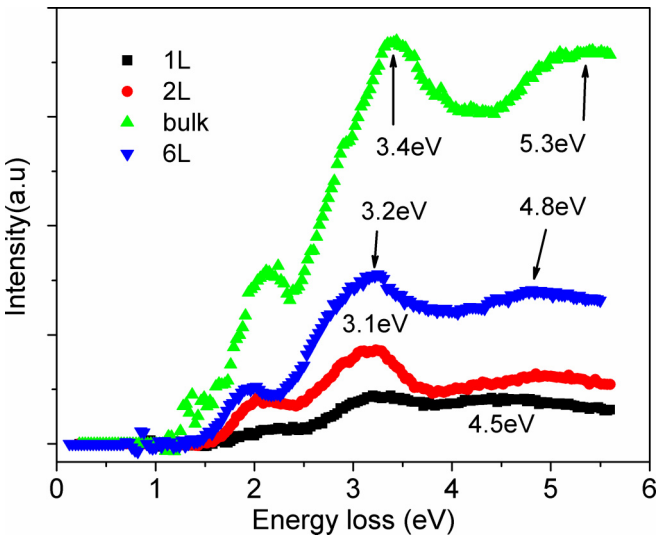

FIG. 4. The fine structures of angle-integrated low-loss spectra revealing interband transitions in MoS_2 with different thicknesses.

over q_x complicates the spectra interpretation as it mixes the in-plane contribution into the $q_y = 0$ spectrum, however, the mixing effect is expected to be negligible as $q_y \gg q_c$. For example, the momentum transfer vector ($\vec{q}$), for the A,B peak centered at 2 eV seen in the $q_y = 0.01$ Å^{-1} spectrum shown in Fig. 2(a), is determined from electron scattering kinetics to be oriented at least as large as 88° from the c axis of the sample. The corresponding angle for the 4 eV loss is also higher than 86°, so that the energy-loss spectrum at $q_y = 0.01$ Å^{-1} over the whole energy range can be interpreted as an in-plane polarized contribution. In general, the mixing of the two polarized contributions is always present but they are expected to show different q_y dependence. For the loss

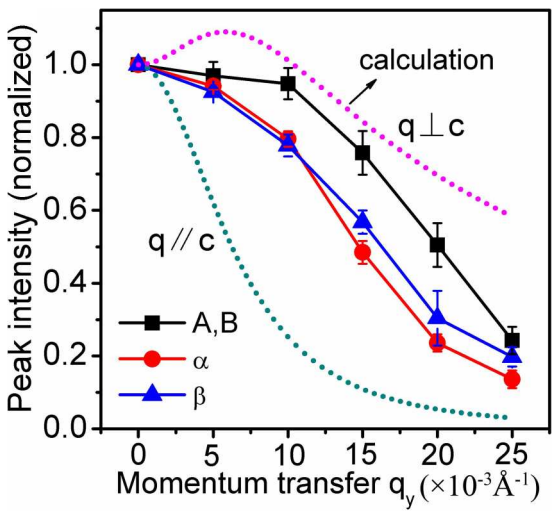

FIG. 5. The relative change of A,B, α, and β peak (at 2, 3.1 and 4.5 eV) intensities with momentum transfer q_y. Peak intensity at q_y is normalized by its counterpart at $q_y = 0$. The experimental data is the case between the pure in-plane mode and the pure out-of-plane mode predicted by the calculation, illustrating that each spectrum should be a linear superposition of these two components.

feature centered at 2 eV, the normalized intensity is initially independent of q_y, in agreement with the expected dependence of the in-plane contribution. On the other hand, the intensities of the broad α,β peaks centered at 3.1 and 4.5 eV drop more rapidly, consistent with the contribution from the out-of-plane excitation which occurs at small momentum transfer.

B. Separation of in-plane and out-of-plane spectral components

Another sign for the strong orientation effect of the dielectric response is the disappearance or appearance of certain characteristic spectral features, such as the δ peak (seen at 3.9 eV), as q_y increases [Fig. 2(a)]. We will make the simple assumption that for the small energy range considered in Fig. 5, the integrated spectra are linear superpositions of the in-plane and out-of-plane components. This is because the integration equation (1) can be seen as a linear superposition of the following two components:

$$I_{\perp} = \mathrm{Im}(\varepsilon_{\perp}) \int_{-\sqrt{q_0^2-q_y^2}}^{\sqrt{q_0^2-q_y^2}} \frac{q_x^2+q_y^2}{\left|a\left(q_x^2+q_y^2\right)+q_E^2\right|^2}\, dq_x \Delta q_y, \quad (2)$$

$$I_{//} = \mathrm{Im}(\varepsilon_{//}) \int_{-\sqrt{q_0^2-q_y^2}}^{\sqrt{q_0^2-q_y^2}} \frac{q_E^2}{\left|a\left(q_x^2+q_y^2\right)+q_E^2\right|^2}\, dq_x \Delta q_y, \quad (3)$$

where $a = \varepsilon_{\perp}/\varepsilon_{//}$ is the relative ratio of in-plane to out-of-plane dielectric constants. These two "pure" components in Fig. 5 (dotted line) can be estimated by calculating Eqs. (2) and (3), where a is taken as a constant (Fig. 10) to simplify the calculation.

Any two experimental spectra I_1 and I_2 at different q_y can be hybridization of $I_{\perp}$ and $I_{//}$ components:

$$\begin{aligned} I_1 &= c_1 I_{\perp} + c_2 I_{//}, \\ I_2 &= c_3 I_{\perp} + c_4 I_{//}. \end{aligned} \quad (4)$$

Through simple subtraction between the "hybridized" experimental spectra (Fig. 2 for monolayer and multilayer), we can solve this matrix equation (4) to obtain pure components $I_{\perp}$ and $I_{//}$, by multiplying a constant c_1/c_3 or c_2/c_4 to the subtracted spectrum I_2. This is similar to the method used by Gu [29] to separate energy-loss near-edge fine structure at the boundary from that in the bulk by a subtraction. Different trial coefficients of c have been multiplied to the subtracted spectrum to yield a series of possible differential spectra as shown in Fig. 6.

The key to avoiding a subjective scaling factor determination is to monitor the abrupt δ feature which seems to be predominantly in the in-plane directions which are detected in the large "q_y" spectra (see Figs. 2 and 3). The sharp δ peak, absent in the small angle, is the sole property of the in-plane contribution. For such sharp spectral feature, inappropriate subtraction will result in unphysically sharp spectral variation (pit) [29] in the difference spectrum, as shown by the arrows in Fig. 6. As the abrupt δ feature should be easily recognizable, we use its absence to determine the most likely out-of-plane component, marked with a red circle in Fig. 6(b).

Based on this insight, we have extracted pure in-plane or out-of-plane transitions in monolayer and multilayer. The appropriateness of the subtraction can be checked by observing the appearance of fine structure of the α peak in the polarization-resolved spectra. In the polarization-resolved spectra, we see that the in-plane spectrum has a double peak (α', α'') structure on the shoulder of the α peak, while the out-of-plane feature has a simple single-peak structure. This provides a simple explanation of the complex behaviors of α', α and α'' peaks in the experimental momentum-dependent spectra as shown in Figs. 2 and 3. The same method is also used in multilayer systems [Figs. 6(c) and 6(d)].

C. Polarization-resolved spectra

Figure 7(a) shows the resulting in-plane and out-of-plane spectral contributions, using the above unbiased numerical processing. Here the out-of-plane ($\vec{q}//c$) components are similar to the electronic transition probed by grazing-incident light with $\vec{E}//c$ polarization, which is quite difficult to explore on atomic layers by optical means because of the transverse nature of the electromagnetic wave.

The polarization-resolved spectra in monolayer MoS_2 immediately suggest that the optical gap in the out-of-plane direction ($E_g^{//}$) has a rather higher value of 2.4 ± 0.2 eV. This means that the direct-gap transition in monolayer seen around 2 eV has an in-plane polarized character. On the other hand, the in-plane and the out-of-plane transitions in the multilayer system near the gap region, which occurs at the smaller energy of 1.5 ± 0.2 eV, seem to have much less obvious polarization dependence, suggesting that the electronic transitions involved in the multilayers have a more 3D-like character.

The peak energies of the three dominant transitions in the energy range of interest, detected in the monolayer MoS_2, display negligible dispersion as shown in Fig. 7(b). As a result, we can ignore the dispersion effect in our discussions of momentum-dependent spectra. The dispersionless character of the A,B peaks is consistent with the excitonic nature of this spin-orbit split direct transition [13]. Theoretically the valence band spin-orbit splitting leads to a 0.15 eV difference between the spin-orbital split states of the excitons [30]. However, the broadening due to phonon scattering and the limited energy resolution of our instrument (0.14 eV) means that we are unable to discriminate these two closely spaced A,B peaks. In fact, the other two sharp transition features we have identified all show negligible variation over the momentum range being probed.

The anisotropic property we have observed may be understood in terms of the electronic orbitals of MoS_2 (Refs. [13,31]) which is typical of transition-metal dichalcogenides, with the $4d$ orbitals of Mo situated within the larger energy σ-σ^* gap of bonding and antibonding s-p orbitals [32,33]. Because of the trigonal prismatic nature of the S ligand atom arrangement, the $4d$ orbitals are further split into bonding e_g-like upper bands involving d_{xz},d_{yz} orbitals and a t_{2g}-like lower band involving d_{z^2}, d_{xy}, and $d_{x^2-y^2}$ orbitals. The hybridization among the symmetry-allowed combination of d orbitals produces the resulting electronic states, but at high symmetry points, it is useful to discuss the states and the electronic transitions in terms of the atomic orbitals involved. *Ab-initio* calculations [27,30,34] have identified the direct band gap as the transition at the K point of the first Brillouin zone which has a predominant Mo $d_{x^2-y^2}$ character, and the indirect energy gap arises from the transition from Γ_v (local valence band

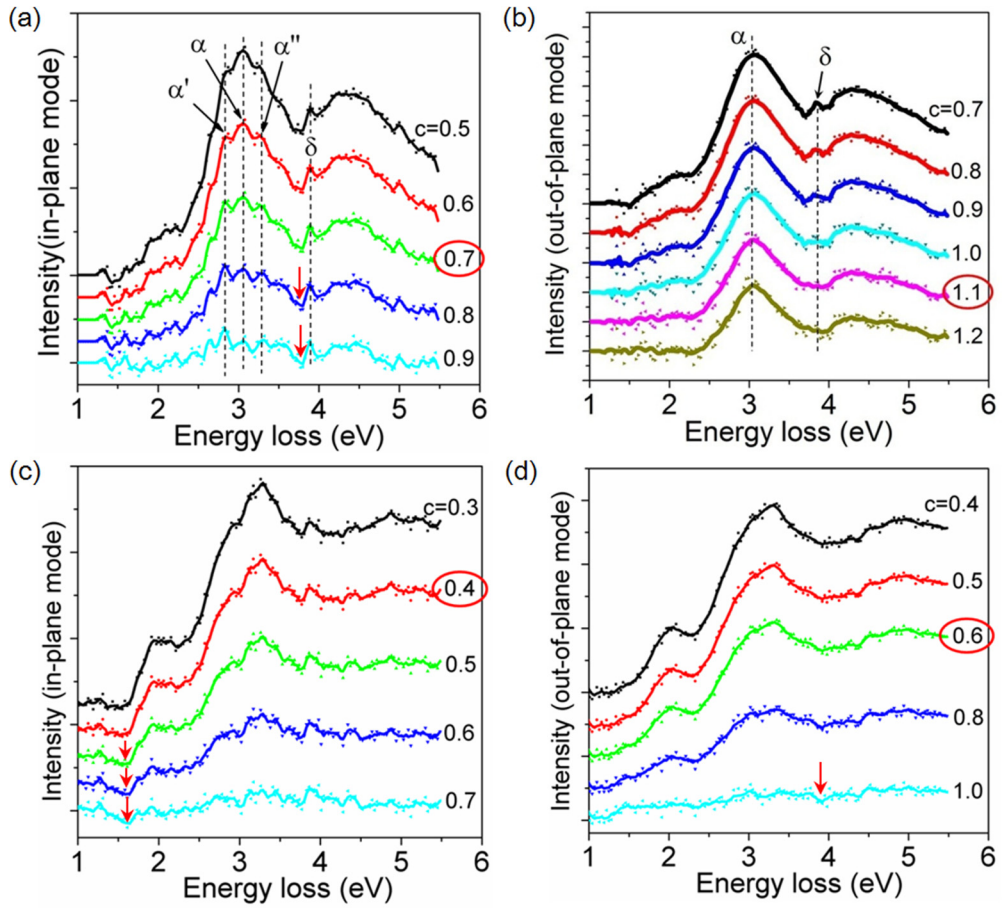

FIG. 6. (a), (b) The possible in-plane and out-of-plane spectral components in monolayer MoS_2, based on the subtraction of two momentum-resolved spectra using suitable subtraction factor c. The optimal subtraction factor marked by red circles ($c = 0.7$ for the in-plane component and 1.1 for the out-of-plane component) is based on the presence or absence of the physically realistic δ feature unique to the in-plane component. It is found that α peaks are split into α', α'' in the in-plane component, while it is a single well-behaved peak in the out-of-plane component. Note that inappropriate subtraction will result in unphysically sharp spectral variation (pit) [29] in the difference spectrum, as shown by the arrows. (c), (d) The in-plane and out-of-plane spectra in multilayer MoS_2, extracted from the original EELS data based on the same subtraction procedure.

maximum at the Γ point) to Q_c [local conduction band valley Q point shown in Fig. 8(b)]. The electronic orbital character of Γ_v has been identified with Mo-d_{z^2}-S-p_z hybrid [32]. The dipole-allowed transition detected by EELS requires a parity change, thus the direct d-d transition at the K point should strictly only be allowed for $\vec{q} \perp c$ polarization as we have

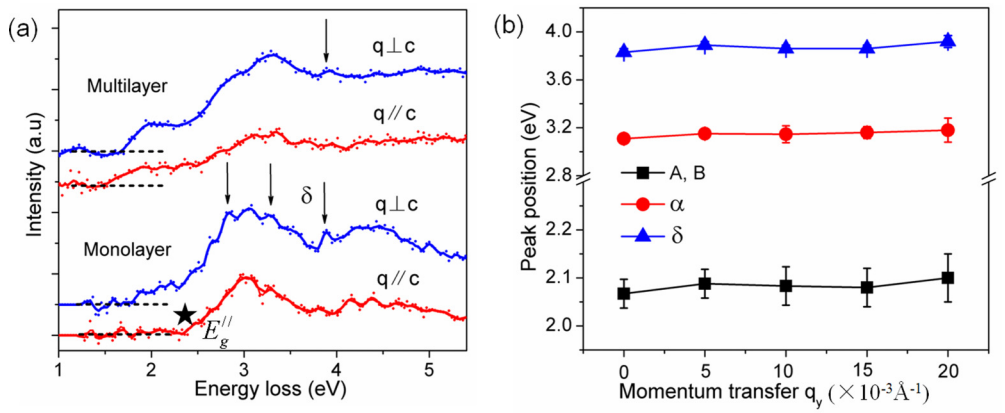

FIG. 7. Polarization dependence of near-gap EELS in atomically thin MoS_2. (a) Absorption spectra of monolayer and multilayer MoS_2 at in-plane ($\vec{q} \perp c$) and out-of-plane ($\vec{q} // c$) polarization. The black star (⋆) indicates the threshold energy (2.4 ± 0.2 eV) in out-of-plane polarization which is inaccessible by optical measurements. (b) Dispersion effect of the peak energy (peak position) of major absorption peaks in Fig. 2(a). All lines are drawn as a visual aid to the trend seen in the data.

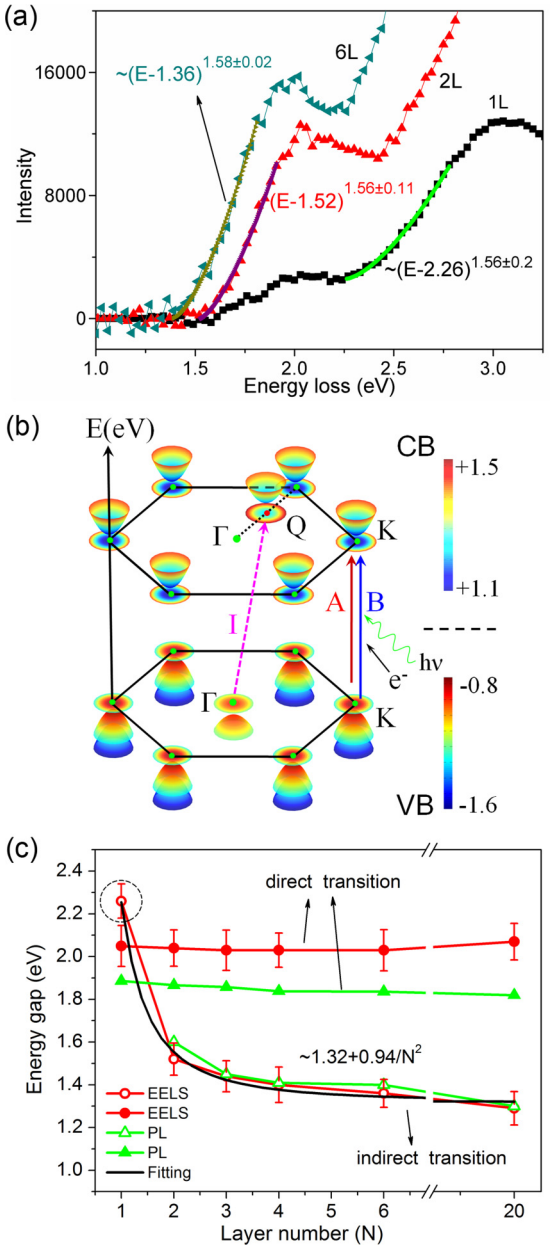

FIG. 8. Dimensionality analysis and quantum confinement effect of electronic transitions. (a) A closer look at band edge transition. Nonlinear fittings of near-gap fine structures give the indirect transition energy ($\Gamma \rightarrow Q$ transition). (b) Schematic illustration of the band structure of monolayer MoS_2 with global conduction band minimum (CBM) and valence band maximum (VBM) both at the K point. The second VBM is located at the Γ point and the second CBM at the Q point (almost midpoint of straight line ΓK). For the sake of brevity, only one Q point paraboloid is drawn (altogether six). The false color disks are the projection of parabolic dispersion to describe the positions of local VBM or CBM. (c) A summarized electronic transition energy between this work and other reports [13,14,34,39]. Note the direct transition energies of different layers are extracted from the peak energy of A,B exciton transitions. The black dashed circle highlights the indirect transition energy in the monolayer system which cannot be easily measured by optical pumping. Nonlinear fitting of indirect transition energies quantitatively confirms the quantum confinement effect.

observed in the monolayer case [Fig. 7(a)] and the indirect transition from Γ_v should only be allowed in $\vec{q}//c$ polarization. Our result for the multilayer suggests that the second selection rule is relaxed.

The nonbonding nature of the $d_{x^2-y^2}$ orbital involved in the threshold transition also means that the monolayer MoS_2 could be a more durable ultrathin photodetector [7,8] as it is less likely to suffer from photobleaching effect. On the other hand, this polarization-specific optical response offers a way to improve the performance of MoS_2-based optoelectronic [3–8] devices in photovoltaics. For example, the out-of-plane dipole transitions in monolayer provide a distinctive possibility to more efficiently utilize the photons above the in-plane-polarized gap 1.8 eV and enhance the photoconversion of solar spectrum possibly engineered through either adjusting interlayer coupling or surface adsorption.

D. Higher energy excitation

The wide energy range covered by the EELS method allows us to easily see the higher energy excitation at 3.1–3.5 eV. This is predicted by the accurate theoretical quasiparticle calculation at the level of GW approximation for the energy level and Bethe-Salpeter equation for the absorption spectrum [27] and has not been observed by the optical method so far. Our analysis also reveals interesting anisotropy. For example, the sharp in-plane δ feature can be associated with the direct in-plane K-K'' excitation from the spin-orbital split valence band maximum to the upper conduction band minimum about the K point. The quasiparticle-excitation calculation of 1H-MoS_2 and few-layer 2H-MoS_2 indicate the α peak at 3.1 eV [Fig. 2(a)] should arise from the transition between the parallel conduction band and valence band around the Q point, where high joint density of states is involved [27]. Interestingly, the α (3 eV) peak structure changes from a single peak in the out-of-plane direction to the split twin peak structure in the in-plane direction. These subtle anisotropy changes are worth further investigation. Nevertheless, the absorption at 3 eV can also be highly efficient because it is not restricted by the anisotropy-imposed selection rules.

E. Dimensionality analysis of joint density-of-states and layer-thickness dependence

Spectral analysis, based on fitting the power law $(E - E_g)^n$ to the angle-integrated spectra, has traditionally been used to determine the character of the near-threshold low-energy absorption. Examples have shown that diamond has an indirect band gap [35] and GaAs has a direct band gap [36]. In arriving at this, Brown and Rafferty have shown that electronic excitation intensity is described as [35]

$$I(E) = \int \frac{d^2\sigma}{dE\, d\Omega} d\Omega = \begin{cases} \mathrm{JDOS}(E) \\ (E - E_g)\mathrm{JDOS}(E) \end{cases}, \qquad (5)$$

where JDOS(E) is the joint density of states. The upper equation in (5) applies for direct transitions, and the lower one for indirect transitions. For the 3D semiconductors, the JDOS for a parabolic dispersion follows $(E - E_g)^{0.5}$. Hence in the 3D case, the intensity for direct transition presents the power law with exponent of $n = 0.5$ and indirect transition $n = 1.5$,

verified experimentally for a number of 3D semiconducting materials. We have extended their argument on the energy dependence of the spectral intensity for direct and indirect transitions in two-dimensional electronic systems where JDOS has an exponent $n = 0$. Hence the corresponding power-law exponents of the spectral analysis should, in principle, be $n = 0$ (direct) and $n = 1$ (indirect), respectively.

We investigate the dimensionality of the JDOS involved through power-law analysis of the spectral variations. The fitted exponents for the threshold transitions in bilayers and multilayers [shown in Fig. 8(a)] are all close to 1.5. Together with the polarization-insensitive energy gap transition shown in Fig. 7(a), they demonstrate that the transition involved has a three-dimensional-like character. The observation of three-dimensional-like dispersion in the few-layer systems (2L, 3L, 6L) is consistent with the strong dispersion of the valence band (dominated by $S - p_z$ states) in the ΓA orientation [31,37] and has previously been understood as interlayer coupling of the $S - p_z$ orbitals across the van der Waals spacing. This 3D-like character is also in accord with the electrostatic screening experiment [38].

We then follow the evolution of the indirect transition as a function of the layer thickness, even after the crossover from indirect-to-direct gap transition [Fig. 8(a)]. This is because the overlapping direct transition in the monolayer system should have a power-law dependence of $(E - E_g)^0$, similar to the JDOS of the two-dimensional character [20] of the band structure near the K point. Although near the threshold, the spectrum does not follow such power law due to the strong excitonic peak [27,39], we expect that such a power-law dependence prevails above the band-gap region where the excitonic effect is absent. Indeed, such a flat absorption band has been well known experimentally in the related TMDs [20]. We therefore identify the rising absorption above direct transition at 2 eV in monolayer with the same transition responsible for the indirect $\Gamma \rightarrow Q$ transition [Fig. 8(b)] in multilayered MoS_2. This identification is supported by recent photoconductivity measurements indicating that the transition in this energy range is associated with excitation into the conduction band at the Q point [40]. Giving support to this identification, the power fitting returns a spectral intensity exponent of 1.56 ± 0.20. The deduced transition energy is 2.26 ± 0.06 eV, corresponding to a 3D-like indirect transition in monolayer, as is the case in the multilayer system. In comparison, the $\Gamma \rightarrow Q$ indirect transition is predicted to be 2.0 ± 0.1 eV from local-density approximation calculation [27,34] and 2.5 ± 0.2 eV from the more accurate quasiparticle calculation [27] in monolayer systems.

The observation of 3D-like JDOS associated with the indirect transition in the monolayer case cannot be explained as interlayer coupling across the van der Waals spacing as it is absent. We suggest that it is because the confinement potential is "soft" in the sense that it rises slowly with the distance from the surfaces. It is well known that if the confinement potential along the out-of-plane direction is abrupt ("hard edge") as found in semiconductor quantum well structures, then we expect the allowed k_z values of the carrier wave functions to take discrete values. If, however, the confinement potential approaches the vacuum level more gradually ("soft edge") as one moves away from the monolayer, then it is possible that the allowed k_z can take quasicontinuous values and JDOS may follow $(E - E_g)^{0.5}$ as it approaches the vacuum level, as in the case of Rydberg atoms.

Our 3D-like JDOS result is consistent with the assumption made by Castellanos-Gomez *et al.* [38] in explaining their electrostatic screening data in monolayer MoS_2. In their study of the electrostatic screening by means of electrostatic force microscopy in combination with a nonlinear Thomas-Fermi theory, they find that a continuum model of decoupled layers, which satisfactorily reproduces the electrostatic screening for graphene and graphite, cannot account for the experimental observations in MoS_2. A three-dimensional model with an interlayer hopping parameter can, on the other hand, successfully account for the observed electric field screening by MoS_2 nanolayers, pointing out the important role of the interlayer coupling in the screening of MoS_2.

F. Thickness-dependent transition energies

The aforementioned three-dimensional nature of the indirect transition provides a logical explanation for the observed strong layer dependence of the threshold energy for the indirect transition. Figure 8(c) summarizes the transition threshold energies in MoS_2 with different thicknesses which are generated from the previous quantitative power-law spectral analysis. Table I compares our EELS-derived transition gap values, the reported photoluminescence and calculation results, with all showing consistent trend with layer thickness. It must

TABLE I. A comparison of energy gaps for both indirect transitions ($\Gamma \rightarrow Q$) and direct transitions ($K \rightarrow K'$) using EELS, PL, or density-functional theory (DFT) methods.

	Indirect energy gap (eV)			Direct energy gap (eV)		
Layers	EELS	PL [13]	DFT [30,41]	EELS	PL [13]	DFT [30,41]
1	2.26 ± 0.11	—[a]	2.1	2.05 ± 0.10	1.89	1.79
2	1.52 ± 0.10	1.60	1.609	2.04 ± 0.08	1.87	1.78
3	1.44 ± 0.10	1.45	1.5	2.03 ± 0.09	1.86	1.76
4	1.40 ± 0.11	1.41	1.3	2.03 ± 0.08	1.84	1.74
6	1.36 ± 0.10	1.40	1.1	2.03 ± 0.09	1.84	1.73
Bulk	1.29 ± 0.09	1.30	0.93	2.07 ± 0.08	1.82	1.73

[a]The energy of the indirect transition in monolayer system is not measurable using PL because it is higher than the energy of the direct-gap transition.

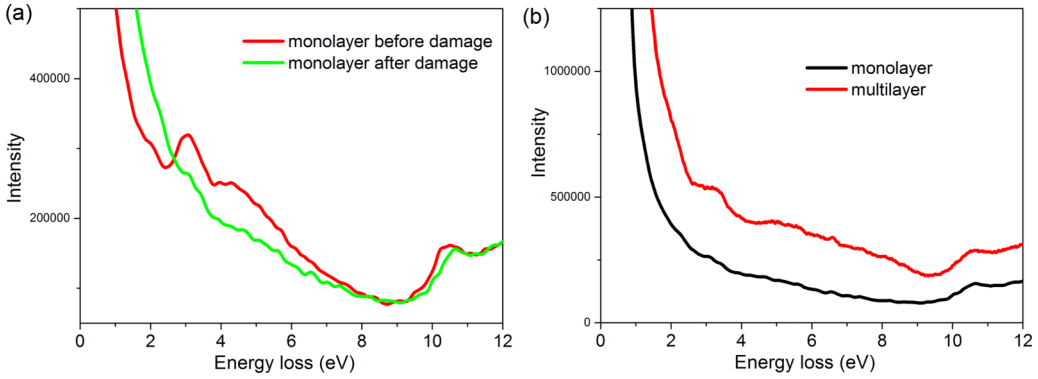

FIG. 9. (a) Low-loss EEL spectra from a fresh MoS_2 monolayer (in red) and that after exposure to electron beam irradiation for 4 h at 60 kV. (b) Low-loss EEL spectra recorded from monolayer and multilayer MoS_2 after extended electron beam irradiation.

be pointed out that the indirect gap of multilayer systems evolves into the direct gap of the monolayer MoS_2, as the number of layers is reduced. However, EELS allows us to track the indirect transition even when its threshold energy is now shifted beyond the direct-gap transition energy. To test independently our assignment of the indirect electronic transitions in the monolayer, we have found that the threshold energy of the indirect transition as a function of the layer number, N, can be fitted by the expression $E_g = E_B + A/N^2$ as shown by the fitting curve in Fig. 8(c). E_B is 1.32 $\pm$ 0.01 eV and corresponds to the indirect gap of bulk MoS_2. The quantitatively well-fitted black line is consistent with the size dependence of the energies in a classic one-dimensional potential well and further verifies the physical picture of quantum confinement effect in layered MoS_2.

Calculations by Molina-Sanchez *et al.* and Kumar and Ahluwalia [27,34] predict a downward shift of the Γ_v point when the thickness is reduced. This has been corroborated by ARPES measurements, although the bandwidth of the valence band is smaller in experiment because of the substrate effect [15]. To date, there is no experimental information about the movement of the conduction band structure. Therefore, we use our determination of the energies for the direct and indirect transitions [in Fig. 8(c)] to map out the movement of the conduction band valley Q_c [Fig. 8(b)]. The ARPES data suggests that the Γ_v point was downward shifted from its bulk value to the case of monolayer by 0.7 eV. From our data, the evolution of the indirect transition energy suggests that the local Q_c point moves upward by a much smaller amount (0.3 eV) comparable with the theoretical calculation [27]. This may arise from different atomic orbital hybridizations: the former Γ_v (mainly Mo-d_{z^2}-S-p_z) is more sensitive to interlayer coupling than the Q_c (d_{z^2} and d_{xy}, $d_{x^2-y^2}$ orbitals). This asymmetry has consequence for many physical properties, such as changes in the effective mass of electrons and holes which are important for the transport in few-layer MoS_2 systems.

G. Effect of radiation damage on EELS fine structures

By comparing the EEL spectra recorded from the monolayer MoS_2 before and after the beam damage as shown in Fig. 9, we found that the irradiation associated with long-term electron beam irradiation could lead to the disappearance of A,B excitons peaked at 2 eV and the strong interband transitions (α and β at 3.1 and 4.5 eV, respectively) in monolayer MoS_2. For multilayer specimens, the beam damage after long-time exposure (about 4 h here) will obviously weaken the fine structures in their EEL spectra. Results from such a comparison here demonstrate that the low-loss fine structures in EEL spectra are mainly coming from the transitions between electronic bands of intact crystals.

V. SUMMARY

In conclusion, we showed that electronic excitation in MoS_2 presents not only the well-known indirect- to direct-gap transition, but also less-anisotropic to highly anisotropic response, as the thickness is reduced to monolayer. The latter favors the optical absorption by normally incident light, and hence may be partially responsible for the enhanced photoabsorption seen in monolayer MoS_2. In particular, the well-known 1.8 eV direct gap in monolayer MoS_2 is shown to be entirely in-plane polarized, consistent with the 2D character of the $d_{x^2-y^2}$-like orbitals involved, while the out-of-plane-polarized energy gap is much larger at 2.4 $\pm$ 0.2 eV. Such an extremely anisotropic optical and electronic property in the monolayer system is important for the development of efficient photovoltaic and photocatalysis applications. It may give rise to a novel interlayer transport property in layer-stacking heterostructures.

We also showed that the joint density of states of the indirect Γ-Q transition is 3D-like in character, even in the monolayer case. We propose that this is due to the soft-edge nature of the confinement potential, which makes the electronic states involved easily tunable by vertical stacking. We showed experimentally that the threshold energies of the indirect Γ-Q transition follow the well-known quantum confinement scaling relationship, in contrast with the layer-thickness independence of the K-K' direct transition. Our investigation presents systematic and comprehensive insight into the physics of this new semiconductor and may also benefit orientation-dependent applications in optoelectronics and heterostructured electronics.

ACKNOWLEDGMENTS

This work is financially supported by the National Basic Research Program of China (Grants No. 2014CB932500 and No. 2015CB921004) and National Science Foundation of China (Grants No. 51222202 and No. 51472215). The research reported in this paper was partially supported by King Abdullah University of Science and Technology (KAUST). J.Y. acknowledges Pao Yu-Kong International Foundation for a visiting Chair Professorship in ZJU and EPSRC and Royal Society for partial support. Dr. Ray Egerton and Dr. He Tian are kindly acknowledged for critical reading, comments, and revisions.

J.H. and K.L. contributed equally to this work.

APPENDIX

The rationality of our assumption that each spectrum can be a linear superposition of these two components is from the observation that the factor "*a*" only appears in the denominator as one of the terms of the two quadratic terms, so the effect of small variation (Fig. 10) of "*a*" as a function of energy over the narrow energy range of interest can be negligible as no strong plasmon resonance is involved.

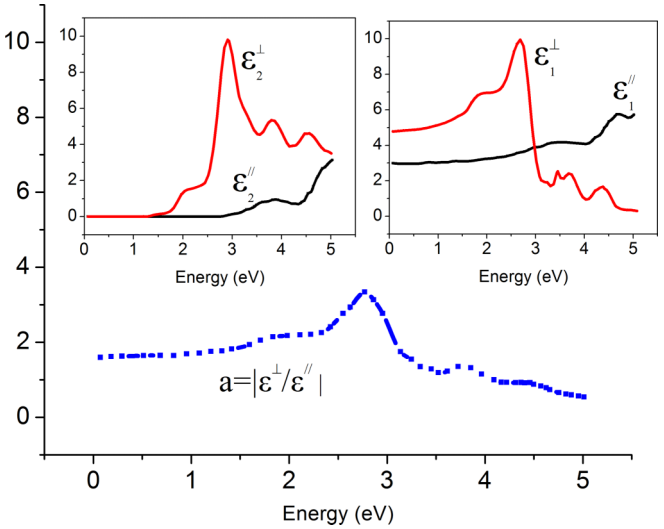

FIG. 10. Dielectric functions and their ratio (*a*); the inset shows dielectric constants extracted from Ref. [34]. It shows small variation of "*a*" as a function of energy.

[1] Q. H. Wang, K. Kalantar-Zadeh, A. Kis, J. N. Coleman, and M. S. Strano, Nat. Nanotechnol. **7**, 699 (2012).

[2] C. Ataca, H. Sahin, and S. Ciraci, J. Phys. Chem. C **116**, 8983 (2012).

[3] Y. Zhang, J. Ye, Y. Matsuhashi, and Y. Iwasa, Nano Lett. **12**, 1136 (2012).

[4] B. Radisavljevic, A. Radenovic, J. Brivio, V. Giacometti, and A. Kis, Nat. Nanotechnol. **6**, 147 (2011).

[5] B. Radisavljevic, M. B. Whitwick, and A. Kis, ACS Nano **5**, 9934 (2011).

[6] B. W. H. Baugher, H. O. H. Churchill, Y. Yang, and P. Jarillo-Herrero, Nano Lett. **13**, 4212 (2013).

[7] Z. Yin, H. Li, H. Li, L. Jiang, Y. Shi, Y. Sun, G. Lu, Q. Zhang, X. Chen, and H. Zhang, ACS Nano **6**, 74 (2012).

[8] H. S. Lee, S. Min, Y. Chang, M. K. Park, T. Nam, H. Kim, J. Kim, S. Ryu, and S. Im, Nano Lett. **12**, 3695 (2012).

[9] H. Zeng, J. Dai, W. Yao, D. Xiao, and X. Cui, Nat. Nanotechnol. **7**, 490 (2012).

[10] K. F. Mak, K. He, J. Shan, and T. F. Heinz, Nat. Nanotechnol. **7**, 494 (2012).

[11] T. Li and G. Galli, J. Phys. Chem. C **111**, 16192 (2007).

[12] S. Lebegue and O. Eriksson, Phys. Rev. B **79**, 115409 (2009).

[13] K. F. Mak, C. Lee, J. Hone, J. Shan, and T. F. Heinz, Phys. Rev. Lett. **105**, 136805 (2010).

[14] A. Splendiani, L. Sun, Y. B. Zhang, T. S. Li, J. Kim, C. Y. Chim, G. Galli, and F. Wang, Nano Lett. **10**, 1271 (2010).

[15] W. Jin, P. C. Yeh, N. Zaki, D. Zhang, J. T. Sadowski, A. Al-Mahboob, A. M. van der Zande, D. A. Chenet, J. I. Dadap, I. P. Herman, P. Sutter, J. Hone, Jr., and R. M. Osgood, Phys. Rev. Lett. **111**, 106801 (2013).

[16] Y. Zhang, T. Chang, B. Zhou, Y. Cui, H. Yan, Z. Liu, F. Schmitt, J. Lee, R. Moore, Y. Chen, H. Lin, H. Jeng, S. Mo, Z. Hussain, A. Bansil, and Z. Shen, Nat. Nanotechnol. **9**, 111 (2014).

[17] A. K. Geim and I. V. Grigorieva, Nature (London) **499**, 419 (2013).

[18] T. Georgiou, R. Jalil, B. D. Belle, L. Britnell, R. V. Gorbachev, S. V. Morozov, Y. J. Kim, A. Gholinia, S. J. Haigh, O. Makarovsky, L. Eaves, L. A. Ponomarenko, A. K. Geim, K. S. Novoselov, and A. Mishchenko, Nat. Nanotechnol. **8**, 100 (2013).

[19] L. Britnell, R. M. Ribeiro, A. Eckmann, R. Jalil, B. D. Belle, A. Mishchenko, Y. J. Kim, R. V. Gorbachev, T. Georgiou, S. V. Morozov, A. N. Grigorenko, A. K. Geim, C. Casiraghi, A. H. Castro Neto, and K. S. Novoselov, Science **340**, 1311 (2013).

[20] W. Liang, J. Phys. C **6**, 551 (1973).

[21] L. Gu, V. Srot, W. Sigle, C. Koch, P. van Aken, F. Scholz, S. B. Thapa, C. Kirchner, M. Jetter, and M. Rühle, Phys. Rev. B **75**, 195214 (2007).

[22] R. Arenal, O. Stephan, M. Kociak, D. Taverna, A. Loiseau, and C. Colliex, Phys. Rev. Lett. **95**, 127601 (2005).

[23] W. Zhou, J. Lee, J. Nanda, S. T. Pantelides, S. J. Pennycook, and J. Idrobo, Nat. Nanotechnol. **7**, 161 (2012).

[24] P. Wachsmuth, R. Hambach, M. K. Kinyanjui, M. Guzzo, G. Benner, and U. Kaiser, Phys. Rev. B **88**, 075433 (2013).

[25] Y. Sun and J. Yuan, Phys. Rev. B **71**, 125109 (2005).

[26] R. F. Egerton, *Electron Energy-Loss Spectroscopy in the Electron Microscope*, 3rd ed. (Plenum, New York, 1996).

[27] A. Molina-Sanchez, D. Sangalli, K. Hummer, A. Marini, and L. Wirtz, Phys. Rev. B **88**, 045412 (2013).

[28] C. von Festenberg, Z. Phys. **227**, 453 (1969).

[29] H. Gu, Ultramicroscopy **76**, 159 (1999).

[30] E. S. Kadantsev and P. Hawrylak, Solid State Commun. **152**, 909 (2012).

[31] T. Böker, R. Severin, A. Müller, C. Janowitz, R. Manzke, D. Voß, P. Krüger, A. Mazur, and J. Pollmann, Phys. Rev. B **64**, 235305 (2001).

[32] L. F. Mattheis, Phys. Rev. B **8**, 3719 (1973).

[33] M. Chhowalla, H. S. Shin, G. Eda, L. Li, K. P. Loh, and H. Zhang, Nat. Chem. **5**, 263 (2013).
[34] A. Kumar and P. K. Ahluwalia, Mater. Chem. Phys. **135**, 755 (2012).
[35] B. Rafferty and L. M. Brown, Phys. Rev. B **58**, 10326 (1998).
[36] P. E. Batson, K. L. Kavanagh, J. M. Woodall, and J. W. Mayer, Phys. Rev. Lett. **57**, 2729 (1986).
[37] R. Coehoorn, C. Haas, J. Dijkstra, C. J. F. Flipse, R. A. de Groot, and A. Wold, Phys. Rev. B **35**, 6195 (1987).
[38] A. Castellanos-Gomez, E. Cappelluti, R. Roldán, Nicolás Agraït, F. Guinea, and G. Rubio-Bollinger, Adv. Mater. **25**, 899 (2013).
[39] R. A. Neville and B. L. Evans, Phys. Status Solidi B **73**, 597 (1976).
[40] D. Kozawa, R. Kumar, A. Carvalho, K. K. Amara, W. Zhao, S. Wang, M. Toh, R. M. Ribeiro, A. H. Castro Neto, K. Matsuda, and G. Eda, Nat. Commun. **5**, 4543 (2014).
[41] A. Kumar and P. K. Ahluwalia, Eur. Phys. J. B **85**, 186 (2012).